

## NSTX FY2010 Year End Report

NSTX successfully completed its FY 2010 plasma campaign on September 24, 2010, meeting or exceeding all its research and facility/diagnostic milestones including the ARRA extended one run week. This was enabled by improved operating efficiency due to the lithium wall conditioning routinely employed. NSTX achieved 15.43 run weeks (target – 15 run weeks) with 2940 plasma shots exceeding the previous record obtained in FY 2009. The average number of plasma shots per week, ~ 190, is nearly a 15% increase from the previous record of 163 shots per week. The NSTX research team conducted over 45 experimental and machine proposals utilizing new facility capabilities, including the Liquid Lithium Divertor and related diagnostic systems, the Beam Emission Spectroscopy diagnostic for low-k turbulence and mode detection, and combined PF4/5 operation for plasma squareness control.

The NSTX research team successfully executed experiments in support of the 2010 DOE Joint milestone: *“Conduct experiments on major fusion facilities to improve understanding of the heat transport in the tokamak scrape-off layer (SOL) plasma, strengthening the basis for projecting divertor conditions in ITER. The divertor heat flux profiles and plasma characteristics in the tokamak scrape-off layer will be measured in multiple devices to investigate the underlying thermal transport processes. The unique characteristics of C-Mod, DIII-D, and NSTX will enable collection of data over a broad range of SOL and divertor parameters (e.g., collisionality  $\nu^*$ , beta  $\beta$ , parallel heat flux  $q_{||}$ , and divertor geometry). Coordinated experiments using common analysis methods will generate a data set that will be compared with theory and simulation.”*

The NSTX contributions to the 2010 Joint Milestone are described in a separate report.

Summary descriptions of the results of research, facility, and diagnostic milestones are provided below. Descriptions of other selected research highlights are also provided. Other NSTX information and statistics such as publications, invited talks, colloquium presentations, awards, and leadership are also reported.

**Research Milestone R(10-1): Assess sustainable beta and disruptivity near and above the ideal no-wall limit. (Target - September 2010. Completed – September 2010)**

**Milestone Description:** Stable and sustained high beta is required for efficient fusion power production in an ST-CTF and burning plasma ST devices. It is also needed for ITER advanced operating scenarios, and future tokamak-based reactors. Results from NSTX and other advanced tokamaks have previously shown that plasma rotation and active mode control can sustain normalized beta,  $\beta_N$ , near and above the ideal no-wall limit. However, disruptions due to resistive wall modes (RWM) and locked neoclassical tearing modes (NTMs) still occur. Disruptions can be triggered when  $\beta_N$  approaches the ideal-

wall stability limit – for example due to a transient confinement improvement, transient loss of rotation, or a transient increase in pressure-profile peaking. To more fully characterize the achievable beta sustainment and disruption avoidance in the ST, mode control improvements will be implemented which may include: (i) application of  $\beta_N$  control via active control of applied neutral beam power, (ii) optimization of present mode control system parameters and RWM sensors, (iii) improvements to the RWM feedback algorithm by implementing advanced state-space control logic, and (iv) real-time feedback on measured resonant field amplification (RFA). The degree to which other instabilities, such as 2/1 NTMs, impact the disruptivity will also be characterized. Motional Stark Effect and enhanced soft X-ray diagnostics will be assessed for detection of disruption-inducing instabilities and for comparison of measured mode characteristics to theory. Codes such as DCON, IPEC, MISK, MARS-K, and VALEN will be used to calculate ideal beta limits, plasma response to 3D fields, and RWM stability and control. The control techniques, diagnostics, and simulation tools to be applied and developed in NSTX will significantly aid in the development of a predictive capability for the sustainable plasma pressure of high-performance ST and tokamak devices.

### Milestone R(10-1) Report:

NSTX advanced operating scenarios have been shown to depend sensitively on the proximity to ideal stability limits for both internal and external instabilities. In particular, with insufficient NBI power and corresponding NBI current drive, the central  $q$  can slowly evolve toward one in the plasma core which can trigger internal kink and tearing instabilities. Also, if the NBI input torque is insufficient, and/or the rotation profile is not appropriate, a resistive wall mode (RWM) can develop, leading eventually to disruption.

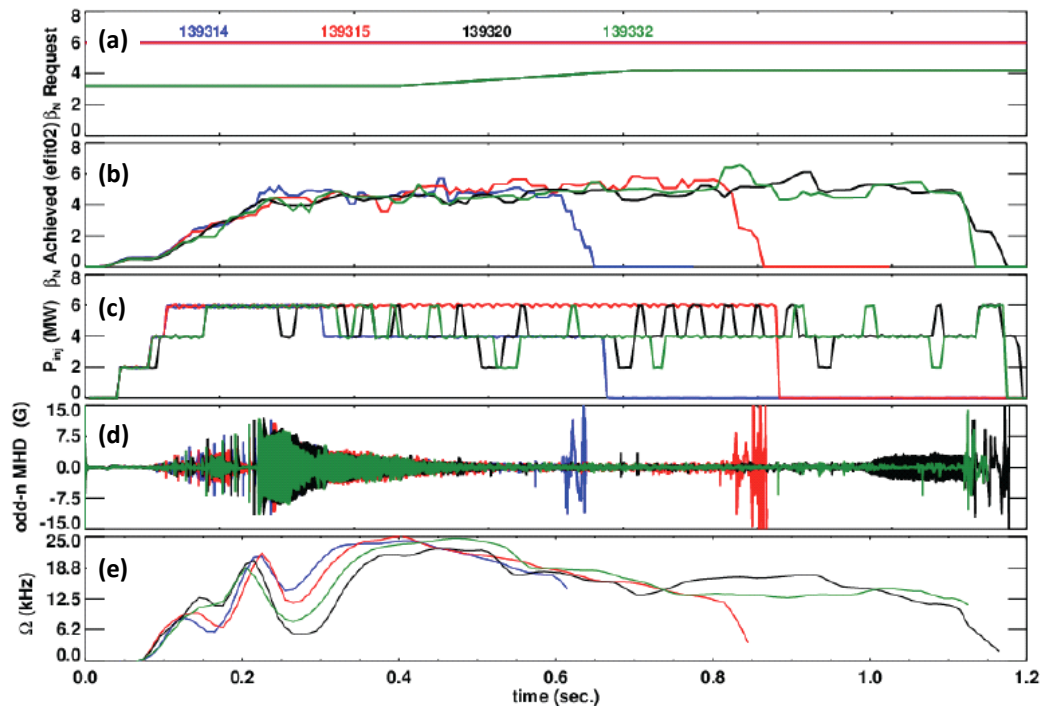


**Figure 1** - (a) Requested  $\beta_N$ , (b) actual  $\beta_N$ , NBI power, odd- $n$  ( $n=1$ ) MHD amplitude, and (e) plasma central rotation frequency during real-time beta feedback control using modulated NBI.

At very high beta, the plasma can also encounter the ideal-wall stability limit which can also induce plasma disruption. However, operation between these two limits enables sustained stable operation in NSTX. Thus, an important tool for disruption avoidance in NSTX is active feedback control to operate with as high beam power and torque as possible without exceeding the ideal-wall stability limit. NSTX has utilized the normalized beta ( $\beta_N$ ) calculated by rt-EFIT in its real-time control system to implement real-time control of the NBI power. As shown in Figure 1, a reference shot (blue) with a power step-down from 6 to 4 MW lasts until 0.6s until it encounters an n=1 RWM instability likely due to insufficient torque and/or un-optimized toroidal rotation. The higher power shot (shown in red) with requested  $\beta_N$  of 6 (%·m·T/MA) lasts longer, but also disrupts when  $\beta_N$  approaches 6 near t = 0.8s. By requesting a lower  $\beta_N$  starting at 3 and ramping to 4.5 later in the shot, sustained excursions in  $\beta_N$  above 5 were avoided. These plasmas last until t = 1.2 s and are limited instead by the available inductive flux.

Full VALEN model computed currents:

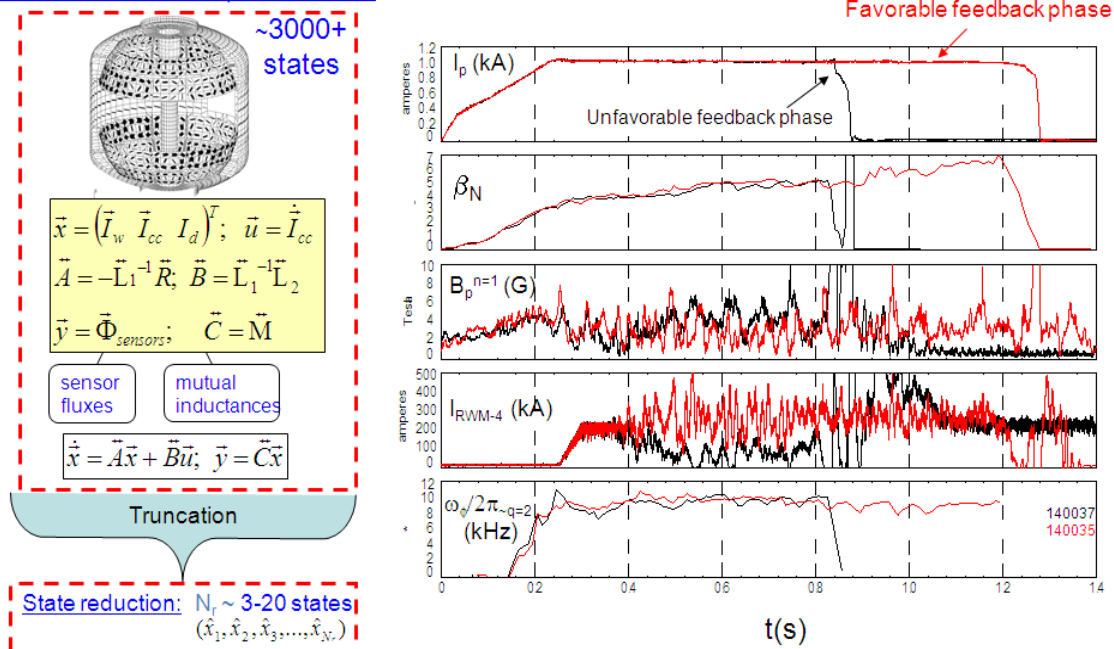


**Figure 2** - (left) Diagram illustrating state-space reduction and (right) comparison of achievable  $\beta_N$  and sustained rotation using unfavorable (black) and favorable (red) feedback phase.

Advanced RWM controllers can further improve performance at high normalized  $\beta$ . RWM controllers used thus far in NSTX have used primarily proportional feedback control. In particular, the externally applied non-axisymmetric radial field is proportional to the measured plasma instability amplitude including a relative phase shift between the measured and applied field. Feedback control can be improved by including models of the electromagnetic properties of the conducting wall responsible for slowing mode growth, and by including the properties of the mode itself. The VALEN code includes both a structure model and a model for the RWM, providing a complete description of the

system to be controlled. However, the ~3000+ states of the VALEN model need to be reduced to a much smaller number of states to enable fast real-time control. This truncation of the possible states to 3 – 20 states is illustrated in Figure 2. The inclusion of 7–10 states is found to adequately capture the dynamic response of the unstable mode, passive structure currents, and sensor signals. Using 7 states, and varying the feedback control phase, clear differences in mode controllability are observed for unfavorable vs. favorable phases as shown in the right-hand plots of Figure 2. With the state-space controller, very high normalized beta plasmas of  $\beta_N = 6-7$  have been accessed. This work represents the first usage of a state-space controller for RWM feedback on any major tokamak facility and should lead to further improvements in sustaining very high beta NSTX plasmas with application to ITER, KSTAR, and next-step facilities.

**FY2010 Research Milestone (R10-2): Characterize HHFW heating, current drive, and current ramp-up in deuterium H-mode plasmas. (Target - September 2010. Completed – September 2010)**

**Milestone Description:** HHFW/ICRF auxiliary heating is expected to be important in next-step STs such as NHTX and ST-CTF as a means of supplementing NBI heating for plasma ramp-up and sustainment. Building on the improved understanding and mitigation of parasitic surface-wave excitation in 2006-2007, the HHFW system on NSTX will be tested as an efficient bulk heating and central current profile control tool in deuterium H-mode plasmas. HHFW has previously produced bootstrap fractions as high as 85% in low-IP H-mode ramp-up plasmas, but was limited by antenna voltage constraints and the deleterious effects of ELMs on RF wave coupling. Antenna upgrades to increase the coupled power and to provide ELM resilience will be implemented to develop bootstrap current overdrive ramp-up of an ST plasma for the first time. The same antenna upgrades will also enable improved electron heating in reduced-density sustained H-mode discharges which could enhance the NBICD (and HHFW-CD) efficiency. Power deposition and current-drive calculations will be performed, and these results will be utilized by the TRANSP code to characterize the heating efficiency, current drive, and transport modifications induced by HHFW. The interaction of HHFW with fast-ions from NBI will be modeled to assess the electron heating efficiency in advanced scenarios with strong NBI heating. Finally, simulations of the plasma current ramp-up will be utilized to understand and optimize current ramp-up with HHFW. Understanding and improving the performance of HHFW/ICRF coupling and heating could significantly reduce the risk of extrapolating RF technologies to next-step STs and ITER.

## Milestone R(10-2) Report:

HHFW research this year focused on coupling RF power into deuterium H-mode plasmas as needed for start-up research and advanced scenarios. Up to 2.1 MW of HHFW power was sustained for up to 200ms with  $k_{\phi} = -8 \text{ m}^{-1}$  (co-current drive phasing). Up to 2.7 MW was sustained for 160 ms, and 2.9 MW for 50ms. For heating phasing ( $k_{\phi} = -13 \text{ m}^{-1}$ ), up to 1.6 MW was coupled into D NBI H-mode. Low current ( $I_p = 300\text{kA}$ ) plasmas were developed to study non-inductive current sustainment using both HHFW and NBI. The interaction of HHFW and NBI heating at this low current was studied systematically for the first time with full diagnostic capabilities available including MSE and FIDA, and it was found that HHFW heating in combination with NBI heating can reliably increase the poloidal beta to high values ( $\beta_p \geq 1.5$ ) and reduce the surface voltage to low values ( $\leq 0.1\text{V}$ ). For fully non-inductive current-drive and ramp-up using HHFW and/or NBI, operation at  $\beta_p = 2-2.5$  is projected to be required.

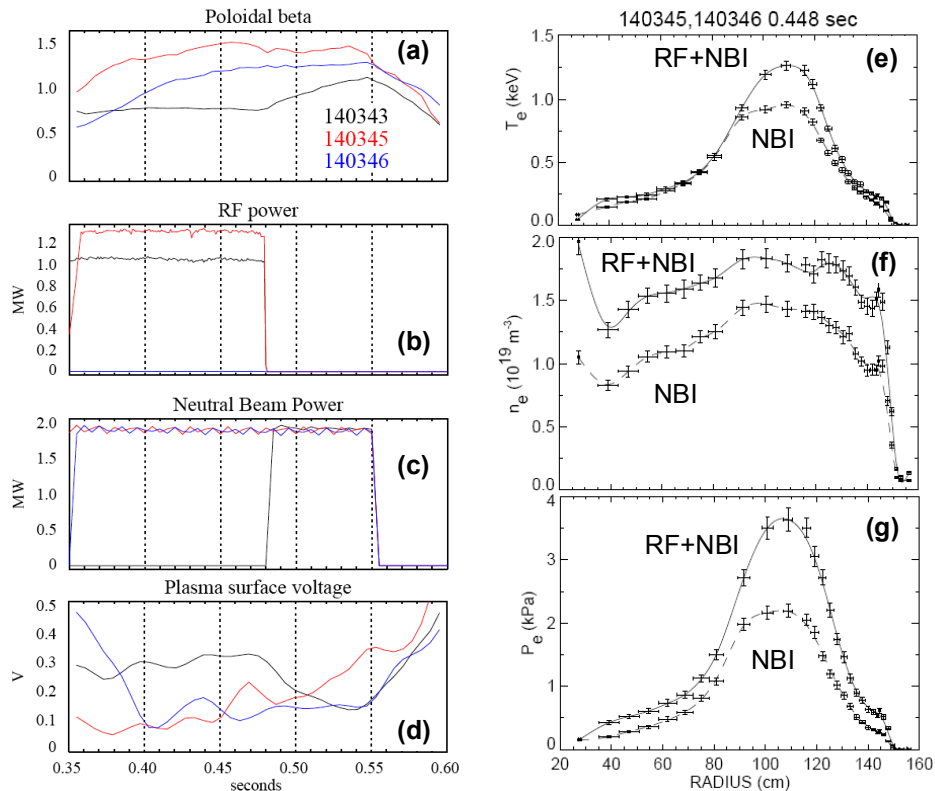


**Figure 3** - (a) Poloidal beta, (b) RF power, (c) NBI power, (d) surface voltage, (e) electron temperature comparison, (f) electron density comparison, and (g) electron pressure comparison for low current ( $I_p=300\text{kA}$ ) target plasmas used for plasma current ramp-up research.

As shown in Figure 3 (black curves in a-d), RF heating at  $\sim 1\text{MW}$  generates  $\beta_p \approx 0.6$ , and  $2\text{MW}$  of NBI alone (immediately following RF turn-off) increases the  $\beta_p$  from  $\sim 0.6$  to  $\sim 1$ . If  $2\text{MW}$  of NBI is used instead  $1\text{MW}$  RF heating (blue traces), the  $\beta_p$  is increased to  $\sim 1.2$ . The combination of  $1.2\text{MW}$  RF +  $2\text{MW}$  of NBI (red traces) produces

higher  $\beta_p = 1.4\text{--}1.5$ . For this combination of RF + NBI, it is evident in Figure 3e-f that the addition of RF increases both the electron temperature and density, and increases the electron pressure by a factor of  $\sim 1.8$ . The H-mode pedestal is prominent in the electron pressure profile, as is strong central peaking of electron temperature and pressure.

As shown in Figure 4, for plasmas in which the HHFW power and NBI power were increased further (1.5MW HHFW + 3MW NBI), preliminary TRANSP analysis indicates  $\sim 60\%$  of the current is sustained non-inductively by bootstrap ( $\sim 40\%$ ) + NBI current drive ( $\sim 20\%$ ). A maximum additional current drive (5-10%) is estimated to be provided by HHFW-CD, resulting in a maximum non-inductive fraction of 65-70% for 300kA target plasmas. Increasing the HHFW power to 3-4MW should substantially increase the bootstrap (to  $\sim 60\%$ ) and RF-driven current fractions to 10-20%, resulting in total projected non-inductive fraction of 80-100%. If the electron temperature cannot be further increased by higher RF power, increased plasma density may increase the bootstrap current as has previously been observed in high non-inductive fraction scenarios at higher plasma current in NSTX.

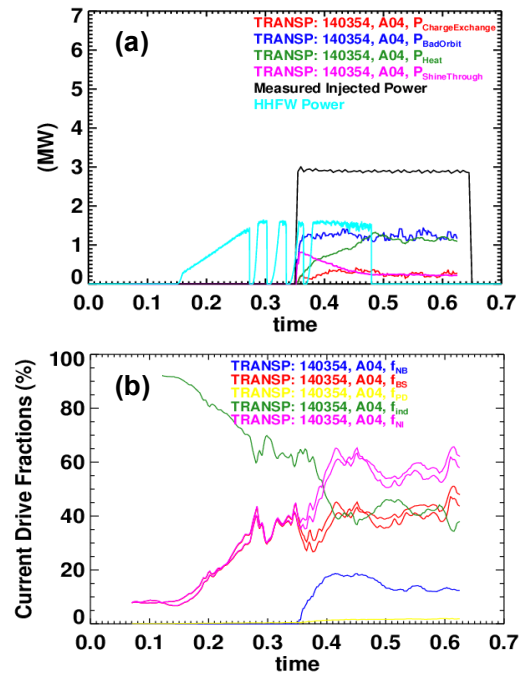


**Figure 4** - (a) Power values, and (b) current drive fractions for HHFW + NBI low  $I_p$  target plasmas.

The RF performance achieved this year is below the  $\sim 4$  MW operation achieved in FY2009. The HHFW research program was constrained in FY2010 by antenna conditioning issues. In particular, at high HHFW power, lithium deposits on the antenna structure, resulting from increased lithium evaporation to load the LLD, were sometimes observed on visible TV images to become mobile during a discharge. If the incandescent globules migrated into the antenna box, they could cause antenna arcs. In addition, unlike all previous NSTX run years, NSTX did not boronize its vacuum vessel components in FY2010 and relied solely on lithium evaporation for wall conditioning. While this worked very well for other operating scenarios on NSTX, it is possible that the lack of boron surface coatings adversely impacted HHFW operation. In addition to developing more routine and extensive vacuum conditioning, the HHFW team is now developing improved shielding/cleaning plans, possibly including modification of boron-nitride limiters surrounding the antenna, improved collimation of the LITER closest to antennas, and the development of a plasma scenario that can “scrub” the antenna surface.

**FY2010 Research Milestone R(10-3): Assess H-mode pedestal characteristics and ELM stability as a function of collisionality and lithium conditioning. (Target - September 2010. Completed – September 2010)**

**Milestone Description:** The high performance scenarios of next-step STs such as NHTX and ST-CTF are based on lower Greenwald density fraction and significantly lower pedestal collisionality than NSTX, which could significantly alter their H-mode pedestal characteristics. Possible differences include deviations from the L-to-H transition threshold power scaling inferred from present ST experiments, different projections for the pedestal height and barrier width, pedestal stability (affecting ELM type and size), and the down-stream divertor plasma and surface conditions, which can also influence the pedestal. Many different ELM regimes have been identified on NSTX, and the dependence of these regimes on collisionality and lithium will be investigated utilizing high-resolution kinetic equilibrium reconstructions coupled to leading linear and non-linear ELM-stability codes to compare to experiments. Pedestal profiles will be compared to kinetic neoclassical predictions to determine if the observed transport is consistent with theory. Particle pumping and density control in these experiments will utilize the liquid lithium divertor (LLD), and a major research focus in this research will be to determine the relative roles of reduced pedestal density and collisionality versus the possible direct effects of lithium. This research will aid development of a predictive capability for pedestal transport and stability limits for the ST, and through comparisons to results from higher aspect ratio tokamaks, will help aid understanding of the role of toroidicity in H-mode confinement.

**Milestone R(10-3) Report:**

A wide range of boundary physics investigations were undertaken in support of the FY2010 research milestone R10-3. Key results include confirmation that the threshold power for the L-H transition depends on X-point radius both with and without lithium coating of the PFCs, and that the threshold power decreases substantially with increased lithium evaporation between shots. As shown in Figure 5, the power threshold (normalized by line-average density) decreased by approximately 40% as the lithium deposited prior to the shot increased from 50mg to 200mg. The threshold power also decreased by 20-30% as the X-point radius was increased from 0.5 to 0.65 m. This dependence of the threshold power on X-point radius is consistent with predictions of the XGC0 code that an increased X-point radius should increase thermal ion orbit loss near the X-point, leading to increased  $E_r$  and  $E_r$  shear near/inside the separatrix. These

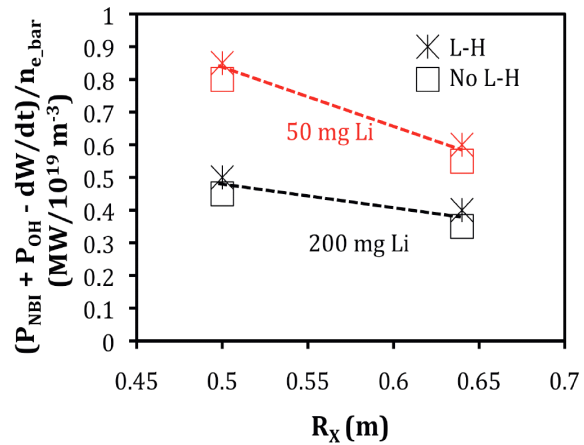


**Figure 5 – L-H transition threshold power versus X-point radius and between-shots lithium.**

are believed to play a role in turbulence suppression and the H-mode threshold power. The mechanism by which lithium coating significantly decreases the threshold power (even when changes in line-average density are accounted for) is unclear, and remains under investigation.

Substantial progress has also been made in modeling the plasma transport and profile response to lithium coatings. Figures 6a and b show the changes in electron density and temperature profiles pre and post lithium wall coating for conditions in which ELMs are eliminated with lithium. The pedestal widths increase by ~100% with lithium wall coatings. These discharges have been modeled with the 2D plasma and neutral code SOLPS. To achieve agreement with the measured profile evolution, it was found to be necessary to both decrease the divertor plate recycling  $R_p$  from 0.98 to 0.92 (constrained by measured divertor  $D_\alpha$ ), and for the cross-field transport coefficients to be reduced substantially across most of the pedestal region and in the SOL. As shown in Figure 6c and d, the effective perpendicular particle transport coefficient  $D_\perp$  (including both pinch and diffusion) decreased by a factor of 4-10 away from the separatrix, and the inferred anomalous electron thermal diffusivity also decreased by a factor of 2-6 inside the separatrix in the pedestal region. The bottom of Figure 6 shows diagrammatically how lithium apparently changes recycling, fueling, and transport to modify the edge profiles in such a way as to suppress edge localized modes.

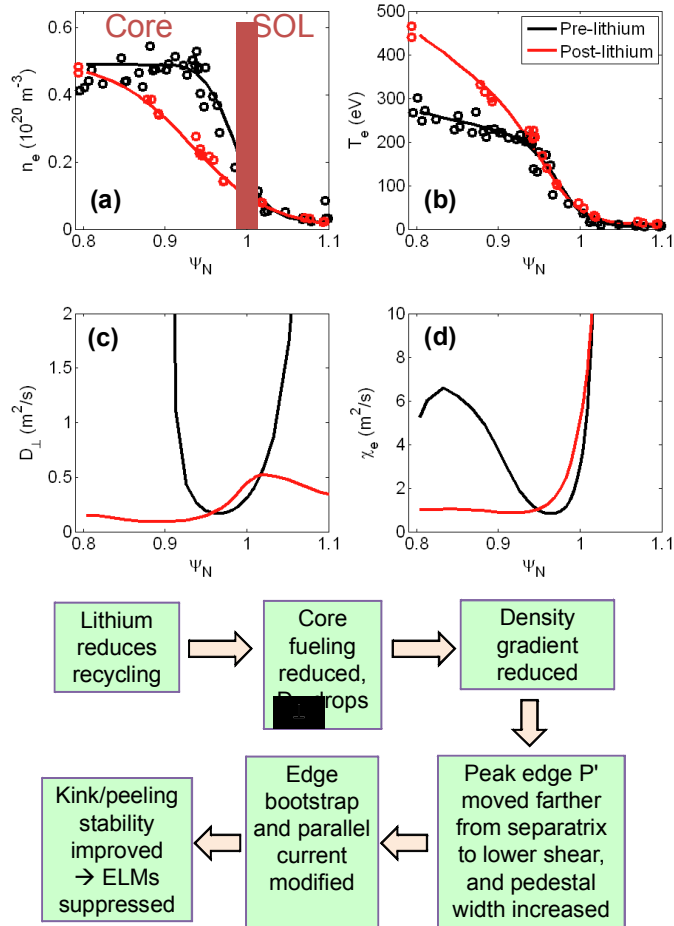


**Figure 6** – (Top) changes in perpendicular particle diffusivity and electron thermal diffusivity pre and post lithium, and (bottom) hypothesized flow-diagram of how lithium modifies pedestal transport and stability.

## **Base Facility and Diagnostics Achievements for FY2010**

NSTX successfully completed its FY 2010 plasma campaign on September 24, 2010, meeting or exceeding all its research and facility/diagnostic milestones including the ARRA extended one run week. This was enabled by improved operating efficiency due to the lithium wall conditioning routinely employed. NSTX achieved 15.43 run weeks (target – 15 run weeks) with 2940 successful plasma shots with 94% operational efficiency. This is the most plasma shots per year, exceeding the previous record number obtained in FY 2009 with more run weeks. The plasma shots per week of ~190 obtained this year is over a 15% increase from the previous record of 163 shots per week achieved in FY 2009. The FY 2010 run started without any boronization for the first time since 2001. The lithium was shown to be effective in controlling the impurity level.

During FY 2010 operations, a water leak was discovered on an OH coil lead. The leak is likely the result of long term (~ 10 years of operations) cyclic stress fatigue due to the thermal growth of the OH coil with respect to the lead support during each discharge. The leak issue was analyzed and the repair procedure was reviewed by external experts. The leak was successfully repaired and an additional support structure was added to minimize the lead area stress. Subsequent monitoring of the area has indicated that the repair has indeed been successful. During the coil repair down time, NSTX has refurbished a failed LITER shutter mechanism with an argon vent. After the vent, the plasma operation was quickly started with lithium. The relatively rapid recovery shows the effectiveness of the argon vent in the lithium environment.

The NSTX team successfully met all facility and diagnostic milestones on or ahead of schedule as noted below. The Liquid Lithium Divertor (LLD) system was commissioned ahead of schedule in collaboration with Sandia Laboratory and other university groups early in the run with the LLD plates were heated up to well above the liquid lithium melting temperature of 180°C. A number of experiments were performed with LLD. The Beam Emission Spectroscopy (BES) system was also commissioned in collaboration with University of Wisconsin in June ahead of schedule and it has already yielded exciting experimental data and has supported a number of experiments.

### **Facility Milestones for FY2010**

**Facility Milestone F(10-1): Operate NSTX Facility for 14 Experimental Run Weeks (Target - September 2010. Completed – September 2010)**

**Milestone Report:** NSTX achieved 14 run weeks with 1705 plasma shots on September 24, 2010.

**Facility Milestone F(10-2): Commission the liquid lithium divertor target system for particle pumping (Target - September 2010. Completed – April 2010)**

**Milestone Description:** Building on the results obtained with the lithium evaporator (LITERS) a liquid lithium divertor target system has been developed and is being deployed on NSTX. While surface reactions limit the effectiveness of the solid lithium surface produced by the lithium evaporator, laboratory measurements indicate that a liquid lithium surface can remain active for continued pumping during high performance, extended discharges. The design, R&D, and major component fabrication for the liquid lithium divertor target were completed in FY2008-2009 and the components were installed in the vacuum vessel in the first quarter of FY2010. It is proposed to utilize the twin lithium evaporator system to apply thin layers of liquid lithium onto the heated LLD surfaces. The LLD system will be commissioned during FY2010 plasma operations.



*Figure 7 – NSTX Liquid Lithium Divertor (LLD) target plates installed in NSTX.*

**Milestone Report:** The NSTX team successfully installed and commissioned the Liquid Lithium Divertor (LLD). During the integrated system test of the LLD, the plates were successfully heated to well above the lithium melting temperature of 180°C. The lithium evaporators (LITERS) were used to apply lithium coating on the LLD plates, before the start of plasma operation and then during the experiments. In total, over 1000 grams of lithium were evaporated into NSTX by the LITER system during FY 2010. Several experiments were conducted to characterize the effects on the plasma of the LLD as a function of the plate temperature and the depth of the lithium applied. The surface temperature of the LLD plates measured by the ORNL two color fast FIR camera system was observed to increase near the plasma strike point.

During the ISTP, however, an electrical fault developed in the heaters of one of the four LLD plates. Further electrical fault problems have occurred in two of the remaining three plates after conducting a series of LLD experiments. The cause of these electrical

failures will be investigated during the upcoming outage. As an alternative to the electrical heaters, a prototype air heater was developed and tested. This succeeded in heating the plate to  $\sim 160^{\circ}\text{C}$  which is close to the lithium melting temperature. A higher power heater will be tested after the current run to confirm that the air-heating system can indeed heat the LLD above the lithium melting point.

### **Diagnostic Milestones for FY2010**

#### **Diagnostic Milestone D(10-1): Commission the Beam Emission Spectroscopy system for transport studies. (Target - September 2010. Completed – June 2010)**

**Milestone Description:** The proposed Beam Emission Spectroscopy (BES) diagnostic on NSTX will enable direct measurements of longer wavelength density fluctuations in the plasma core, providing valuable insights into the suppression of ion turbulence and the attainment of near-neoclassical ion confinement on NSTX. The BES diagnostic together with the existing microwave tangential scattering diagnostic (which measures medium to short wavelength turbulence) will provide the most comprehensive turbulence diagnostic set of any ST in the world. The BES diagnostic should also enhance measurements of the spatial structure of fast-ion-driven instabilities such as the TAE and BAAE observed on NSTX. The design of the BES system builds on the research and development already performed on the DIII-D tokamak by the University of Wisconsin group. The BES system will be commissioned during FY2010 plasma operations.

**Milestone Report:** A collaborative research program between the University of Wisconsin-Madison and NSTX successfully commissioned a beam emission spectroscopy (BES) diagnostic system on NSTX in June 2010. The system measures Doppler-shifted  $D_{\alpha}$  emission from neutral heating beams. 56 fiber bundles were installed in two high throughput optical views centered at  $R = 130$  and  $140$  cm, as shown in Fig. 8. The sightlines sample most of the minor radius ( $0.2 < r/a < 1.0$ ). The system presently operates with 16 detection channels, and detector modules and control systems are available to implement an additional 16 channels for the beginning of the NSTX FY2011 run campaign. All new ultra-low-noise high frequency detector electronics and associated control systems have been developed at UW and implemented in the NSTX BES system to optimize signal quality and allow for full remote operability. These include modern surface-mount components, and low-capacitance, high quantum-efficiency photodiodes. Initial data has been acquired. The signal levels exhibit the expected magnitude, and the signal-to-noise ratio looks promising to determine long wavelength ( $k_{\perp} \rho_i < 1$ ) density fluctuations for physics studies in the areas of turbulence and transport, energetic-particle-driven modes, MHD, and boundary physics. The system has been used in approximately 25 experiments in FY2010 utilizing both optical views. The data show clear signatures of density fluctuations arising from broadband turbulence, energetic-particle-driven Alfvén eigenmodes, MHD, and ELMs and changes in fluctuations are evident at L-H transitions.

## BES together with high-k to provide a comprehensive turbulence diagnostic set

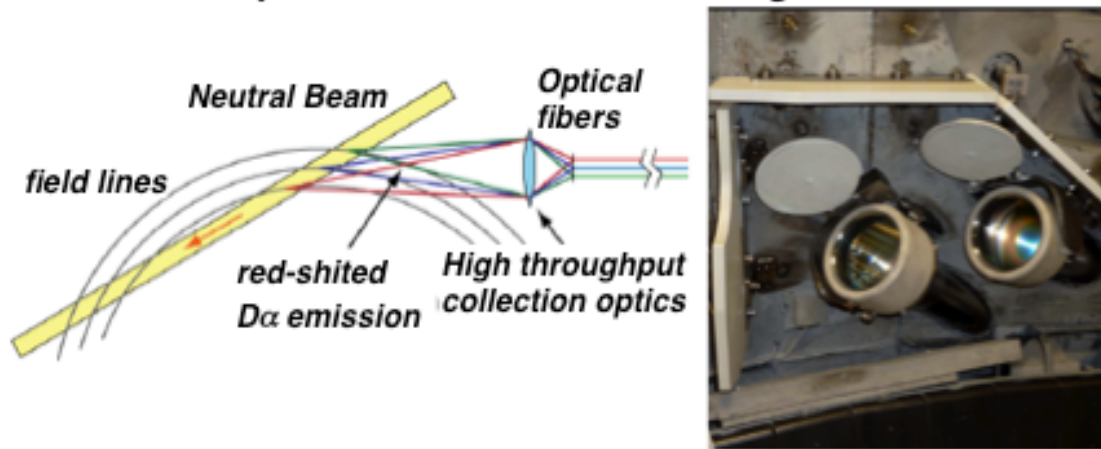


*Figure 8 – NSTX Beam Emission Spectroscopy (BES) diagnostic installed in NSTX.*

### **ARRA Facility and Diagnostics Achievements for FY2010**

Funding provided under the American Recovery and Reconstruction Act 2009 (ARRA) enabled the NSTX facility to operate 1 additional week in FY2010 to enhance the science output particularly in the area of LLD and boundary physics. The ARRA also funded diagnostic upgrades including extra channels for the multi-pulse Thomson scattering (MPTS) system and the Motional Stark Effect Laser-Induced Fluorescence (MSE-LIF) advanced diagnostic system. The MPTS upgrade will improve spatial resolution in the H-mode pedestal and plasma edge to support the FY2011 Joint Research Milestone. The MSE-LIF diagnostic will provide internal magnetic and electric field measurements which will also contribute to the FY2011 Joint Research Milestone. The facility upgrades include an enhancement to the lithium liquid divertor (LLD) capability for improved divertor pumping to control edge collisionality for the FY2011 Joint Research Milestone, a second switching power amplifier (SPA) to provide flexible spatial spectra of the applied 3-D field perturbations to control error fields, resistive wall modes and resonant magnetic perturbation which will contribute to the FY2011 Joint Research Milestone. The LLD related diagnostics enhancement include a plasma material interaction (PMI) probe for in-situ surface analyses of plasma surfaces, a divertor imaging spectrometer for divertor impurity measurements, a Lyman-Alpha ( $Ly_a$ ) detector array for measuring divertor recycling, fast visible cameras for LLD surface monitoring, and a high-density ( $3 \times 33$ ) Langmuir probe array for divertor particle and temperature profile measurements. All of the planned FY 2010 ARRA tasks were completed on or ahead of schedule.

## **ARRA Facility Milestones for FY2010**

### **ARRA Facility Milestone AF(10-1): Operate NSTX Facility for 1 Additional Experimental Run Weeks (Target - September 2010. Completed – April 2010)**

**Milestone Report:** NSTX achieved 1.01 run weeks with 171 plasma shots on April 14, 2010.

### **ARRA Facility Milestone AF(10-2): Complete engineering design of facility upgrades including cost and schedule. (Target - June 2010. Completed – June 2010)**

**Milestone Description:** The present SPAs provide three independently controllable currents to the EF/RWM/RMP coil set. These coils are currently configured through a patch panel, usually to generate perturbations with either the odd ( $n = 1, 3$ ) or even ( $n = 2$ ) toroidal harmonics, although other configurations which include higher field harmonics are also possible, such as one simulating a “missing” control coil to provide data for ITER. However, maximum flexibility will be achieved by installing an additional 3-channel SPA so that each coil is separately powered, allowing simultaneous control of the full range of field harmonics. The design of the additional SPA system will be completed in FY2010.

**Milestone Report:** The engineering design of the SPA upgrade was completed in June 2010. The procurement of the SPA upgrade components has been completed and the components were delivered to PPPL. The installation of the SPA upgrade has begun and the system is on schedule to be commissioned prior to the FY 2011 plasma operation in the spring of 2011.

### **ARRA Diagnostic Milestone AD(10-1): Complete key component procurements and begin assembly of plasma diagnostic upgrades. (Target - June 2010. Completed – June 2010)**

**Milestone Description:** The diagnostic upgrades include extra channels for the multi-pulse Thomson scattering system for improved H-mode pedestal and plasma edge spatial resolution and the Motional Stark Effect Laser-Induced Fluorescence (MSE-LIF) advanced diagnostic system for internal magnetic and electric field measurements. Key components will be procured and assembly will begin in FY2010 for the system to be commissioned in FY2011.

**Milestone Report:** The key component procurements were completed, the component assembly is progressing well, and the components are scheduled to be ready for final installation during the NSTX outage which is scheduled to begin in November 2010. All the ARRA diagnostic systems are scheduled to be available for the FY 2011 run.

## Additional NSTX Achievements in FY 2010:

Beyond the successful completion of the FY2010 research, facility, and diagnostic milestones described above, several additional important scientific and operational results were achieved during the FY2010 run and are described briefly below.

### Increased flux savings from Coaxial Helicity Injection (CHI)

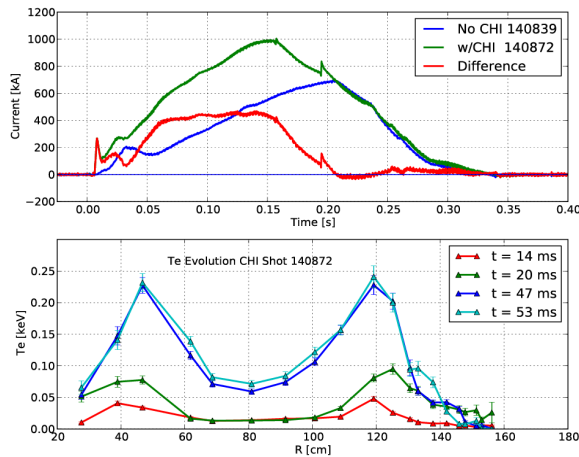


**Figure 9** – (Top) Plasma initiated with CHI and coupled to induction (green) which reaches 1MA at 150ms, comparison discharge that uses the same loop voltage programming, but does not use CHI start-up assist achieves 600kA at the same time (blue), and difference between the two discharges (red). (Bottom) Shown are the electron temperature profiles at various times. The CHI discharge is initiated at 6ms.

The FY2010 CHI experiments focused on maximizing the flux savings at high plasma current following plasma initiation using CHI. In FY2009, up to 800 kA of plasma current was achieved using 100% of the flux from a single swing of the central solenoid. In FY2010, plasma currents up to 1 MA were obtained using only 75% of the inductive flux from a single swing of the solenoid. This is the highest level of current ever produced in NSTX using this level of solenoid flux, and represents a substantial improvement over results obtained in FY2009. This improvement is the result of several factors. First, the

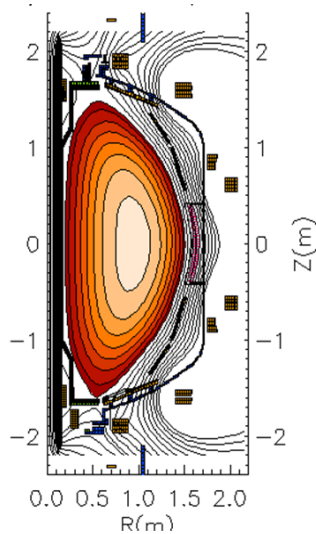


**Figure 10** – EFIT reconstruction for shot 140872 at 100ms.

current in the absorber coils (first used in FY2009) was increased and was extended in duration to reduce absorber arcs. The increased use of lithium coatings also further reduced impurities and associated radiation power losses. Lastly, the injector flux was adjusted to keep the plasma near the injector for a longer time, and the time duration of voltage application was also increased. The coupling of CHI-initiated plasmas to induction without absorber arcs was possible with up to 5 capacitors in FY2010 (versus 3 capacitors in FY2009). Absorber-arc-free operation was also obtained with operation using up to 7 capacitors, but due to limited run time and the exhaustion of the lithium evaporators during the final run day, these higher current discharges have not yet been coupled to induction. Figure 9 is a comparison of two discharges, one with CHI start-up coupled to induction and the second with induction only.

Another important improvement in FY2010 was an increase in electron temperature of up to 100 eV measured 14 ms after the start of the CHI discharge ( $t = 20$  ms in Figure 9) during the transition to induction. The shots with the highest temperature at this time showed the best inductive ramp-up. Previously, in a good CHI discharge, the electron temperature reached 100 eV at 50 ms. The most recent CHI discharges at a similar time reach nearly 250 eV. Another feature of the CHI-initiated discharges is the hollow electron temperature profile which is beneficial for achieving low plasma internal inductance, and this characteristic is retained during the current ramp. Figure 10 shows an equilibrium reconstruction at  $t = 100$  ms which indicates high boundary elongation of  $\sim 2.6$  and very low internal inductance of  $\sim 0.3$  (compared to typical values of 0.4-0.5) which is maintained throughout the current-ramp.

### NBI current profile modifications induced by Alfvénic instabilities

In FY2009, fast-ion transport resulting from the wave-particle interaction between multiple simultaneous Alfvén-Eigenmode (AE) instabilities and the NBI fast-ion population (commonly called an “avalanche”) was studied as an important process that could impact the fusion performance of next-step STs and ITER burning plasmas. Data was obtained to extend previous studies of fast-ion redistribution and loss to explore the effects of fast-ion transport on the equilibrium current profile evolution. In FY2010, the TRANSP analysis of these plasmas has been completed and the effect of large AE avalanches quantified with respect to fast-ion transport and modifications to the beam-driven current profile. Within TRANSP, the fast-ion transport is modeled as anomalous fast-

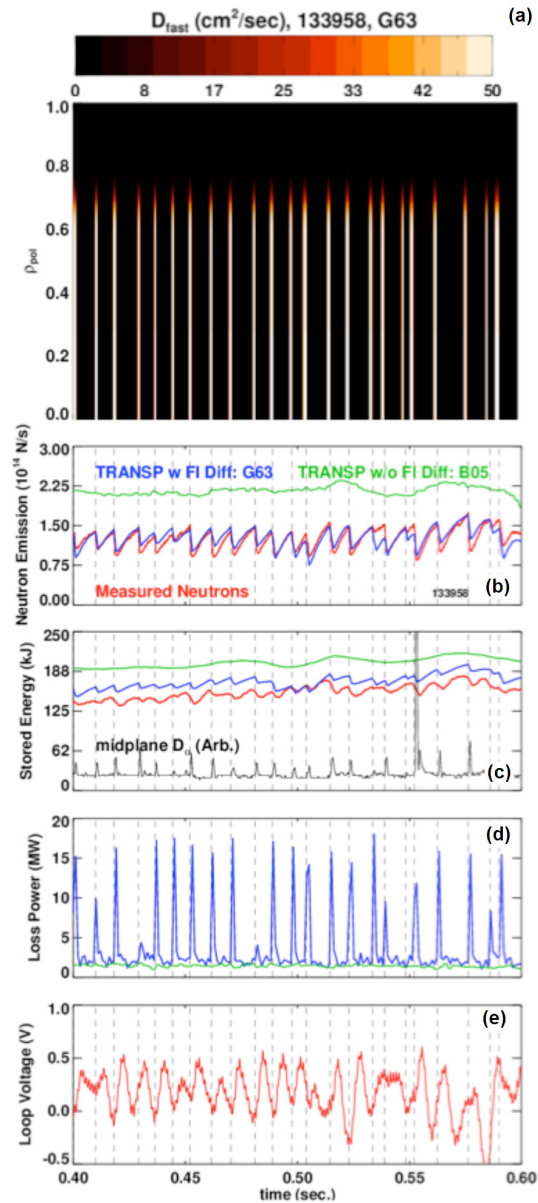


**Figure 11** – a) Imposed fast ion diffusion profile evolution, time traces of b) the neutron evolution, c) the stored energy, d) the calculated fast ion loss power, and e) the loop voltage. In each case, the measurement is indicated in red, a TRANSP simulation without fast ion diffusion is shown in green, and a TRANSP simulation with impulsive fast ion diffusion is shown in blue.

ion diffusion, and the following formula was used to model the spatial and temporal dependence of the diffusivity:

$$D_{FI}(\rho_{pol}, t) = \frac{A_{FI}(t)}{2} \left[ 1 - \tanh\left(\frac{\rho_{pol} - 0.05}{w}\right) \right] + D_{FI,DC}$$

The temporal variation of AFI(t) in the above equation was set by associating the start time and duration of the measured modes to the start time and duration of periods with large AFI. For this experimentally determined timing, scans were done of the radial width (w) and peak amplitude of the fast ion diffusivity “bursts”. The optimal combination of radial width and amplitude would match the average level of the neutron emission, the amplitude of the loss at each mode, and the recovery rate of the neutrons between the modes. Note that for a given TRANSP run, the width and amplitude of these impulsive diffusion phases was identical, and only the timing set to match the data. Also, no effort was made to match the neutron rate drop for each mode; rather the width and amplitude were set to match the neutron drop of a typical mode. The fast ion diffusivity was either set to zero or a small number for periods between the large “spikes”. An example DFI profile in radius and time is shown in Figure 11a. The radial width of the DFI in this case is 0.7 with a peak value of 50 m<sup>2</sup>/s and a steady value between pulses (DFI, DC) of 1 m<sup>2</sup>/sec. Including the impulsive diffusivity improves the match between the calculated and the experimental values of the neutron rate (Fig. 11b) and the total stored energy (Fig. 11c). Figure 11d shows the instantaneous loss power from the bursts. Finally, Figure 11e shows the changes in loop voltage from the changes in fast-ion confinement and NBI current drive.

Figure 12 shows that as a result of the AE impulsive diffusivity, the profile of NBI driven current (red) is strongly modified, and when the anomalous diffusion is included (Figure 12b), the predicted total current density profile (green) is in much better agreement with the reconstructed total current density profile (black).

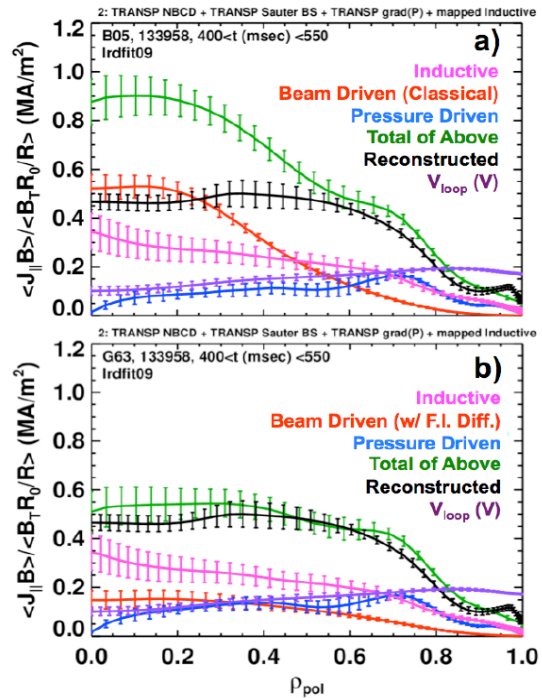


**Figure 12** – Comparison of the current profile reconstruction, using a) classical collisional slowing-down only, and b) the impulsive anomalous diffusivity that matches the observed neutron rate modulations and stored energy.

## First demonstration of boundary “squareness” modification in NSTX

During the initial design of NSTX it was discovered that the original PF4 vertical field coils were predicted to cause a distortion (“dimple”) of the plasma boundary – especially in high beta plasma scenarios, and that this modification could reduce the ballooning stability in the edge region of NSTX plasmas. This prediction motivated the construction and incorporation of the PF5 vertical field coil with increased major radius and reduced vertical separation. The PF5 coil has been used to provide the vertical field in NSTX ever since. In FY2010, the PF4 and PF5 coils were used together in high performance plasma scenarios for the first time. The usage of these coils together has two motivations: 1) to provide the ability to vary the plasma “squareness” as a possible means of modifying the edge transport and stability, and 2) to assess the possibility of combining PF4 + PF5 to provide the vertical field required for 2MA plasmas in NSTX Upgrade without upgrading the PF5 power supplies (thereby reducing the cost of the Upgrade). Figure 13 shows the conventional PF5-only shape (purple) compared to a PF4 + PF5 shape (black) with a power supply current ratio  $I_{PF4} / I_{PF5} = 1.2-1.4$ . The inclusion of PF4 current at a level comparable to or higher than PF5 current reduces the boundary outboard squareness by -0.05 to -0.1. Analysis indicates that the pedestal profiles and stability are not strongly impacted by the boundary shape change. This level of PF4 current exceeds what is needed for the Upgrade ( $I_{PF4} / I_{PF5} \sim 0.5$ ) indicating that the combination of PF4 + PF5 should be able to provide the vertical field needed for a broad range of 2MA plasmas in NSTX Upgrade.

This prediction motivated the construction and incorporation of the PF5 vertical field coil with increased major radius and reduced vertical separation. The PF5 coil has been used to provide the vertical field in NSTX ever since. In FY2010, the PF4 and PF5 coils were used together in high performance plasma scenarios for the first time. The usage of these coils together has two motivations: 1) to provide the ability to vary the plasma “squareness” as a possible means of modifying the edge transport and stability, and 2) to assess the possibility of combining PF4 + PF5 to provide the vertical field required for 2MA plasmas in NSTX Upgrade without upgrading the PF5 power supplies (thereby reducing the cost of the Upgrade). Figure 13 shows the conventional PF5-only shape (purple) compared to a PF4 + PF5 shape (black) with a power supply current ratio  $I_{PF4} / I_{PF5} = 1.2-1.4$ . The inclusion of PF4 current at a level comparable to or higher than PF5 current reduces the boundary outboard squareness by -0.05 to -0.1. Analysis indicates that the pedestal profiles and stability are not strongly impacted by the boundary shape change. This level of PF4 current exceeds what is needed for the Upgrade ( $I_{PF4} / I_{PF5} \sim 0.5$ ) indicating that the combination of PF4 + PF5 should be able to provide the vertical field needed for a broad range of 2MA plasmas in NSTX Upgrade.

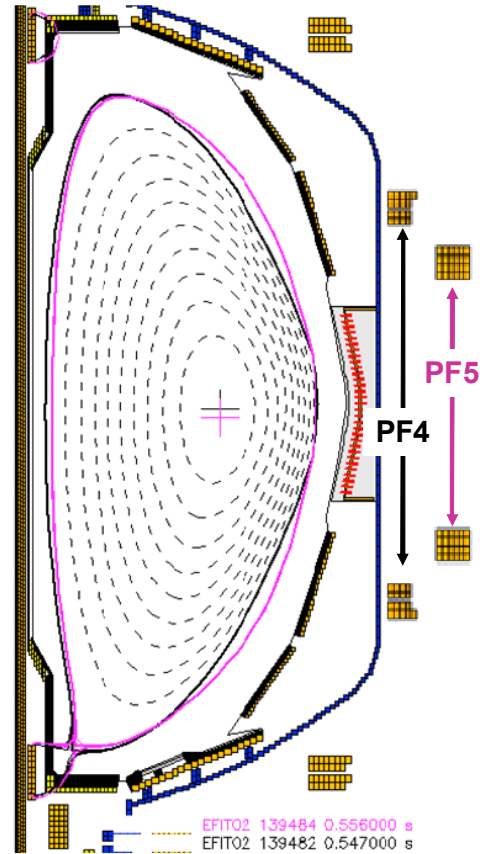
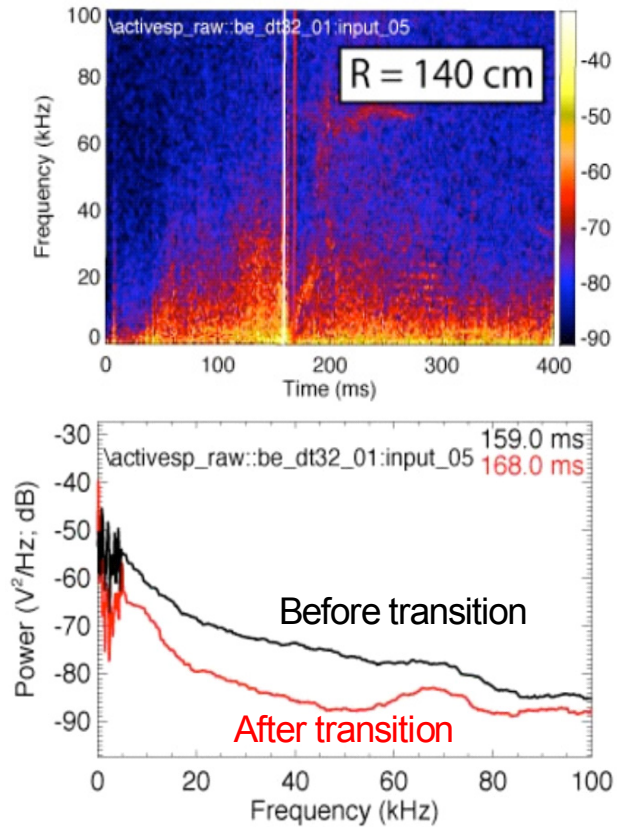


Figure 13 – Comparison of plasma boundaries for PF5 only (purple) and PF4 + PF5 (black).

The inclusion of PF4 current at a level comparable to or higher than PF5 current reduces the boundary outboard squareness by -0.05 to -0.1. Analysis indicates that the pedestal profiles and stability are not strongly impacted by the boundary shape change. This level of PF4 current exceeds what is needed for the Upgrade ( $I_{PF4} / I_{PF5} \sim 0.5$ ) indicating that the combination of PF4 + PF5 should be able to provide the vertical field needed for a broad range of 2MA plasmas in NSTX Upgrade.

## First turbulence data from the Beam Emission Spectroscopy (BES) diagnostic

The BES diagnostic was commissioned in FY2010 as described previously in this report. The BES diagnostic has already produced important turbulence data and is ready to support the turbulence measurement NSTX research milestone planned for FY2011 and the joint research target on core turbulence planned for FY2012. As shown in Figure 14a, the BES diagnostic has measured broad-band fluctuations in the range from zero to 100kHz, with the large fluctuation amplitudes at frequencies less than 50kHz for near-edge radial positions of  $R=1.4$  m. Turbulence measurements have been made before and after the transition to H-mode. As shown in the Figure 14b, there is a significant drop in fluctuation amplitude ( $\sim 10$ dB in power) following the H-mode transition. Not shown are even larger amplitude decreases observed at larger major radius ( $R=1.45$  m), and smaller turbulence amplitude decreases observed deeper in the plasma core ( $R=1.28$  m). Thus, following the H-mode transition, the BES diagnostic data indicates long wavelength turbulence is observed to decrease across the entire radial profile, but the relative decrease is much larger near the plasma edge – consistent with H-mode confinement trends observed previously in NSTX.



**Figure 14** – (Top) frequency spectrogram of raw BES data versus time including an H-mode transition near  $t=160$ ms. (Bottom) BES fluctuation amplitude before and after the H-mode transition.

## NSTX Research in Support of ITER:

The H-mode pedestal height is a critical parameter that will in large measure determine the fusion gain of ITER. Initial NSTX FY2010 experiments performed to better understand the H-mode pedestal structure revealed several important trends. First, it was observed that the pedestal pressure increases by a factor of  $\sim 3$  before the ELM crash and exhibits no consistent indications of pressure saturation. This trend is evident in Figure 15a which shows that for 1MA and 1.2MA plasmas, the total pedestal pressure increases roughly monotonically during the ELM cycle. As shown in Figure 15b, the pedestal height (pressure at top of pedestal) exhibits a strong  $I_p$  scaling with the pedestal poloidal beta varying as  $I_p^{3.6-4.6}$  and the pedestal stored energy  $W_{ped}$  varying as  $I_p^{1.6-2.6}$ . This pedestal stored energy scaling is consistent with ITER-98 scaling which varies as  $W_{ped} \propto I_p^{1.58}$ . As shown in Figure 15c, the electron temperature gradient is weakly dependent on plasma current, whereas the density gradient varies more strongly with current and apparently largely determines the increase in pressure gradient with plasma current. While there is little change in the temperature gradient, the temperature profile does indicate evidence of a localized depletion of the top of the pedestal as a result of the ELM crash. Overall, this pedestal profile dataset and related analysis provides a strong basis for contributing to the FY2011 joint research milestone on pedestal structure.

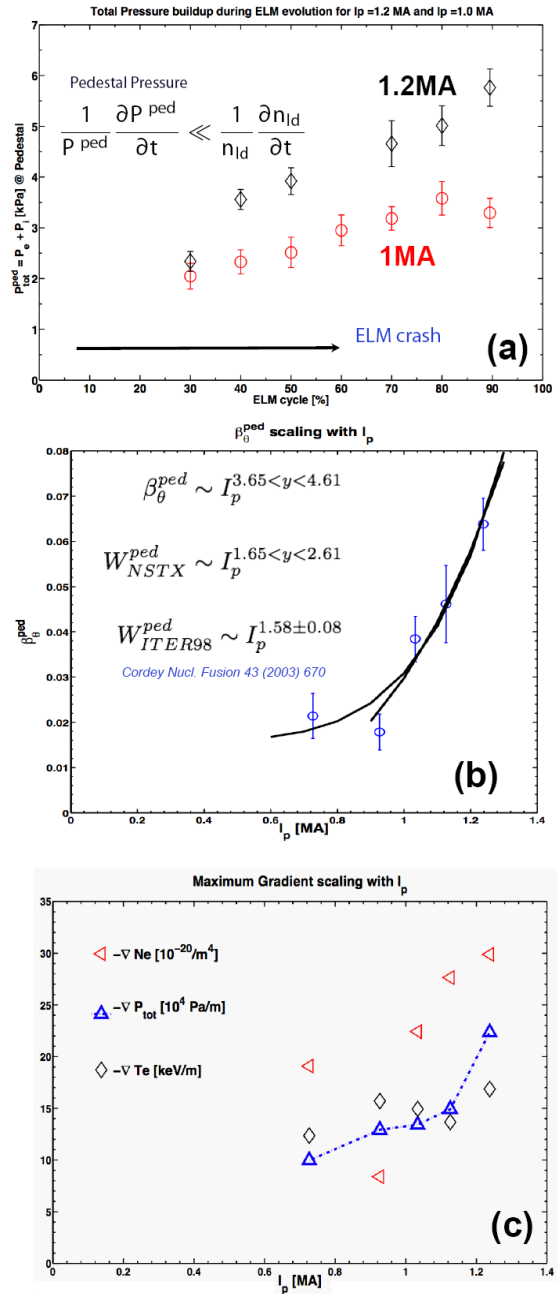


**Figure 15** – (a) Total pedestal pressure vs. relative time during ELM cycle, (b) pedestal height scaling versus  $I_p$ , and (c) gradient of density, pressure, and density versus  $I_p$ .

## Initial results from LLD operation

Thus far, little additional pumping by the LLD has been observed using standard NSTX divertor configurations for either cold or heated LLD plates. However, by focusing plasma exhaust onto the LLD plates by using low flux expansion lower single null plasmas, the first substantial modifications of NSTX H-mode particle evolution were observed. With high incident plasma heat flux, the LLD surface temperature was increased from shot-to-shot and spanned a temperature range from below the melting point of lithium (180C) to temperatures above the melting point. Figure 16a shows the radially and inter-ELM averaged LLD surface temperature  $T_{LDD}$  (on the x-axis) increased from 160C to 300C over the course of 10-15 shots. As the LLD surface temperature increased above  $\sim 200$ -220C, additional fueling was required to maintain an MHD-stable density evolution. As shown in Figure 16a, the ratio of the plasma electron number  $N_{e,plasma}$  to electron source from fueling  $N_{e,fueling}$  decreased by nearly a factor of 2 as  $T_{LDD}$  rose to 250-300C. As shown in Figure 16b, the volume-average electron density is 20% lower when  $T_{LDD}$  is at its highest value even though the fueling is 50% higher for these discharges. Interestingly, Figure 16c shows that the carbon  $Z_{eff}$  is also reduced for the plasmas with elevated  $T_{LDD}$ . Finally, Figure 16d shows that the fraction of LLD surface area above the lithium melting point increases from  $\sim 40\%$  to  $\sim 80\%$  for the plasmas exhibiting electron density and carbon impurity reduction associated with increased  $T_{LDD}$ . These results may indicate that sufficient incident plasma heat and particle flux is needed to condition the LLD porous Mo surface and/or the lithium within the LLD. Additional analysis of the local divertor response (recycling, Li emission, incident ion flux) to strong plasma heating of the LLD is ongoing.

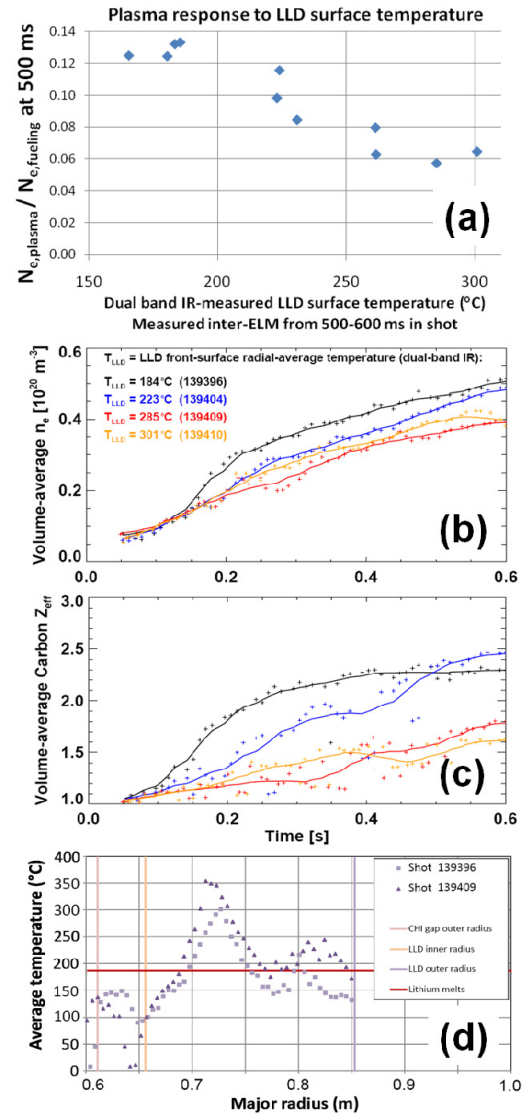


**Figure 16** – (a) Ratio of plasma electrons to total electrons from fueling vs. radial-average LLD surface temperature ( $T_{LDD}$ ), (b) electron density and (c) carbon  $Z_{eff}$  vs. time and  $T_{LDD}$ , (d) local LLD surface temperature vs.  $R$ .